JOURNAL OF GEOPHYSICAL RESEARCH, VOL. ???, XXXX, DOI:10.1029/,

Quasi-biennial oscillation of the ionospheric wind dynamo

Yosuke Yamazaki[1], Huixin Liu[2,3], Yang-Yi Sun[2], Yasunobu Miyoshi[2,3],

Michael J. Kosch[1,4,5], and Martin G. Mlynczak[6]

Correspondence to: Y. Yamazaki (y.yamazaki@lancaster.ac.uk)

[1]Department of Physics, Lancaster University, Lancaster, UK

[2]Department of Earth and Planetary Sciences, Kyushu University, Fukuoka, Japan

[3]International Center for Space Weather Research and Education, Kyushu University, Fukuoka, Japan

[4]South African National Space Agency, Hermanus, South Africa

[5]Department of Physics, University of Western Cape, Bellville, South Africa

[6]NASA Langley Research Center, Hampton, Virginia

Abstract.

The interannual variation of the ionospheric solar-quiet (S_q) current system is examined. A dense magnetometer network over Japan enables the accurate determination of the central position of the northern S_q current loop, or the S_q current focus, during 1999–2015. It is found that the S_q focus latitude undergoes an interannual variation of $\pm 2^\circ$ with a period of approximately 28 months, similar to the quasi-biennial oscillation (QBO) in the tropical lower stratosphere. The QBO-like variation of S_q is particularly evident during 2005–2013. No corresponding interannual variability is found in solar extreme ultraviolet radiation. Comparisons with tidal winds, derived from a whole-atmosphere model, reveal that the QBO-like variation of the S_q current focus is highly correlated with the amplitude variations of migrating and non-migrating diurnal tides in the lower thermosphere. The results suggest that the stratospheric QBO can influence the ionospheric wind dynamo through the QBO modulation of tides.

1. Introduction

Solar-quiet (S_q) daily variations of the geomagnetic field are primarily due to electric currents flowing in the dynamo region of the ionosphere (95–150 km) [see a review by *Yamazaki and Maute*, 2016]. In the dynamo region, the neutral wind $\mathbf{U}$ moves the electrically conducting ionosphere across Earth's main magnetic field $\mathbf{B}$, which produces an electromotive force $\mathbf{U} \times \mathbf{B}$. The associated current density $\mathbf{J}$ can be expressed as:

$$\mathbf{J} = \hat{\sigma} \cdot (\mathbf{E} + \mathbf{U} \times \mathbf{B}), \tag{1}$$

where $\hat{\sigma}$ is the ionospheric conductivity tensor and $\mathbf{E}$ is electric field. The neutral wind at dynamo region heights is dominated by atmospheric tides. The dynamo action by those tides leads to the formation of a global-scale ionospheric current system, which is often referred to as S_q current system. A typical pattern of the dayside S_q current system is illustrated in Figure 1a. The S_q current system is normally comprised of a counterclockwise vortex in the Northern Hemisphere and a clockwise vortex in the Southern Hemisphere. The S_q current system effectively disappears during nighttime because of low ionospheric conductivities.

The strength and shape of the S_q current system change on various time scales. The day-to-day and hour-to-hour variations are mostly due to the variability of atmospheric tides and other waves that propagate into the dynamo region from the lower layers of the atmosphere [*Kawano-Sasaki and Miyahara*, 2008; *Yamazaki et al.*, 2016]. An extreme example of the meteorological impact on the S_q current system can be found during major stratospheric sudden warming events [*Yamazaki et al.*, 2012a,b]. The S_q current system also shows seasonal variability [*Takeda*, 2002; *C*hulliat et al., 2016], which is due to the effects of both ionospheric conductivity and neutral wind. On longer time scales, the solar cycle effect dominates the variability of the S_q current intensity. The S_q current intensity during solar maximum is higher than during solar minimum by a factor of two or so owing to enhanced ionospheric conductivities [*Takeda*, 1999; 2013].

The present study focuses on the interannual variation of the S_q current system. Recent numerical studies showed that the interannual variation of atmospheric tides in the lower thermosphere could be affected by the quasi-biennial oscillation (QBO) [*Liu*, 2014; *Gan et al.*, 2014] and the El Niño Southern Oscillation (ENSO) [*Pedatella and Liu*, 2012, 2013]. The question remains whether the QBO and ENSO have any measurable impact on the ionosphere. This study aims to find out the importance of these meteorological sources in producing interannual variability in the ionospheric electrodynamics. We examine the S_q current system, which is a direct consequence of the ionospheric wind dynamo in the lower thermosphere.

The year-to-year variation of the S_q current intensity is primarily controlled by solar activity, which makes it difficult to detect small changes caused by atmospheric tides. We instead examine the latitudinal position of the S_q current focus. By "S_q current focus", we mean the center of the S_q current loop (see Figure 1a). The accurate determination of the S_q current focus is important in this study, which will be achieved by using a dense magnetometer network over Japan. The latitudinal position of the S_q current focus is not sensitive to solar activity [*Yamazaki et al.*, 2011] and its variability is not well understood.

2. Data and Model

2.1. Geomagnetic data

Ground-based magnetometer data are obtained from 14 Japanese observatories; three stations are operated by the Japan Meteorological Agency and 11 stations by the Geospatial Information Authority of Japan. Figure 1b shows the location of the observatories. We first use the horizontal intensity (H) and the declination angle (D) of the geomagnetic field. The H-component geomagnetic disturbances associated with the magnetospheric ring current are corrected by subtracting the Dst index multiplied by $\cos\theta_m$, where θ_m is the magnetic latitude. The corrected H field is denoted as H_c. The northward (X) and eastward (Y) components of the geomagnetic field are then derived from H_c and D. The magnetic perturbations due to the S_q current system can be derived by subtracting the nighttime baseline, under the assumption that S_q currents are negligible during nighttime due to low ionospheric conductivities. The magnetic perturbations in X and Y are designated as ΔX and ΔY, respectively, which will be used to determine the latitudinal position of the Northern-Hemisphere S_q current focus.

For the determination of the S_q focus position, we basically follow the technique recommended by *Stening et al.* [2005]. This technique requires ΔX and ΔY data from a north-south chain of magnetometers at mid-latitudes where the S_q current focus usually appears. It relies on the fact that both ΔX and ΔY become zero under the focus of the S_q current system. The application of the technique involves the following two steps: (1) determine the time when ΔY crosses the zero level and (2) plot ΔX at that time as a function of latitude to find the latitude where ΔX is zero. We determine the S_q focus latitude on the monthly basis. We first calculate the average daily variations $\overline{\Delta X}$ and

$\overline{\Delta Y}$ for each month using the ΔX and ΔY data corresponding to the ten quietest days of the month. We then apply the technique described above to $\overline{\Delta X}$ and $\overline{\Delta Y}$. The ten quietest days are routinely selected and published by GFZ German Research Centre for Geosciences.

Figure 2 gives an example illustrating the procedures for determining the S_q focus latitude using the Japanese magnetometer data. Figures 2a and 2b show the average daily variations $\overline{\Delta X}$ and $\overline{\Delta Y}$ for February 2001. Different colors indicate different stations. It can be seen from Figure 2b that the time for zero-crossing in $\overline{\Delta Y}$ is around 1200 LT in this case. The $\overline{\Delta X}$ data show both positive and negative perturbations around the noon, indicating that the S_q current focus is located within the latitudinal range of the Japanese magnetometer array. As can be seen in Figure 2c, the $\overline{\Delta X}$ values corresponding to $\overline{\Delta Y}$=0 smoothly changes with latitudes, from positive values at lower latitudes to negative values at higher latitudes. The latitude where $\overline{\Delta X}$=0 gives the S_q focus latitude. We used the polynomial function of degree n=3 for the latitudinal interpolation of the $\overline{\Delta X}$ data. The 1-σ error in the S_q focus latitude was estimated by propagating uncertainty in the nighttime base line of X though the fitting process for determining the latitude of $\overline{\Delta X}$=0. The S_q focus latitude was derived for each month from January 1999 through December 2015.

2.2. GAIA

We examine the interannual variability of tides in the dynamo region using the Ground-to-topside model of Atmosphere and Ionosphere for Aeronomy (GAIA). GAIA is a coupled atmosphere-ionosphere model extending from the ground to the exobase [e.g., *Jin et al.*, 2011; *Miyoshi et al.*, 2012; *Liu et al.*, 2013]. The model consists of physical equations appropriate for various atmospheric processes in the troposphere, stratosphere, mesosphere, and thermosphere under the assumption of hydrostatic equilibrium. The horizontal resolution of the model is 2.8° in longitude and latitude, and the vertical resolution is 0.2 scale height.

We performed a long-term GAIA simulation from January 1996 through March 2016. Following *Jin et al.* [2012], the lower part of the model, below 30 km, was constrained on the basis of a nudging technique using the Japanese 25-year Meteorological Reanalysis [*Onogi et al.*, 2007]. This acts as external forcing that drives the QBO and ENSO in the model, along with other short-term and long-term atmospheric variability. The model also takes into account the variable energetic solar radiation. The $F10.7$ solar activity index was used as a proxy of the solar EUV/UV, which is the primary heat source of the upper atmosphere. The model was run under geomagnetically quiet conditions for the entire duration of the simulation.

Neutral temperature, zonal and meridional winds were output for the altitude range of 100–150 km, corresponding to the dynamo region. Following *Forbes et al.* [2008], a tide was defined in the following form:

$$A_{n,s} \cos\left(n\Omega t + s\lambda - \phi_{n,s}\right), \tag{2}$$

where $A_{n,s}$ and $\phi_{n,s}$ are the amplitude and phase, t is the time, Ω is the rotation rate of the Earth, λ is the longitude. n is a subharmonics of a day. n =1, 2, 3 correspond to oscillations with periods of 24h, 12h, and 8h, and are referred to as diurnal, semidiurnal, and terdiurnal tides, respectively. s is the zonal wavenumber, indicating eastward-propagating waves when s<0 and westward-propagating waves when s>0. The Fourier decomposition technique [*Forbes et al.*, 2008] enables to determine the amplitude and phase of tides with different combinations of n and s. We examine the amplitudes of the migrating diurnal tide (n=1, s=1), non-migrating diurnal tide with zonal wave number 3 (n=1, s=-3), and migrating semidiurnal tide (n=2, s=2). In the rest of the paper, these tides are referred to as $DW1$, $DE3$, and $SW2$, respectively. $DW1$, $DE3$, and $SW2$ are known to have particularly large amplitudes in the dynamo region [e.g., *Oberheide et al.*, 2011], thus have a potential to influence the S_q current system.

For the validation of the tides simulated by GAIA, $DW1$, $DE3$, and $SW2$ in the temperature field at 100 km altitude are compared with those derived from the Sounding of the Atmosphere using Broadband Emission Radiometry (SABER) instrument [*Remsberg et al.*, 2008] onboard the Thermosphere Ionosphere Mesosphere Energetics Dynamics (TIMED) satellite. The model-data comparison will be presented in Section 3.2.

Although GAIA solves for electric fields and currents in the ionosphere, the model does not calculate the magnetic perturbations associated with the ionospheric currents, which are necessary for the determination of the S_q focus position. Thus, we do not conduct model-data comparisons for S_q. The purpose of using GAIA is to derive the interannual variability of tidal winds in the dynamo region, which we will compare with the observed S_q variability.

3. Results

3.1. S_q focus latitude

Figure 3a shows monthly values of the S_q focus latitude over Japan from 1999 through 2015. The average latitude is 30.7°N, in agreement with previous studies [e.g., *Stening et al.*, 2007]. The variations in the S_q focus latitude are much greater than the estimated 1-σ error. The S_q focus latitude occasionally exhibits a large northward displacement beyond

40°N. Such events occurred in February of 2006, 2008, and 2013. As will be seen later, these variations are in part due to the seasonal cycle superposed on the effect of QBO.

The average seasonal variation of the S_q focus latitude during 1999–2015 is presented in Figure 3b. The results show a rapid northward motion of the S_q current focus from January to February. The S_q current focus latitude is lowest during September, and it shows a secondary peak in November. These seasonal characteristics are largely consistent with those presented by *Vichare* [2016] for the Indo-Russian region. The driving mechanism for the seasonal variation of the S_q focus latitude is not well understood. The ionospheric conductivity at middle latitudes is generally highest during local summer and lowest during local winter, which does not explain a complex seasonal pattern of the S_q focus latitude. *Takeda* [1990] and *Kawano-Sasaki and Miyahara* [2008] numerically showed that changes in the thermospheric winds can affect the latitudinal position of the S_q current focus.

The anomaly in the S_q focus latitude was calculated by subtracting the average seasonal variation (Figure 3b) from the original monthly data (Figure 3a). In Figure 4a, the black line shows monthly values of the S_q focus latitude anomaly, revealing fluctuations on a time scale of a few months. The blue and red lines show the smoothed values calculated by applying 7-month and 13-month moving windows, respectively. The two results are in good agreement, indicating that the results are not very sensitive to the choice of the smoothing window. It can be clearly seen that the S_q focus latitude oscillates by approximately $\pm 2°$ on interannual time scales. The interannual variation is most evident during 2005–2013, which roughly corresponds to low solar flux periods.

Figure 4b shows the monthly mean zonal wind measured at Singapore (1.2°N, 103.6°E), which represents the stratospheric QBO. The wind data, extended from *Naujokat* [1986], are provided by Freie Universität Berlin (FUB). The observations cover the region from 70 hPa (∼18 km) to 10 hPa (∼31 km), where the QBO is most prominent. It can be seen that the interannual variation of the S_q focus latitude correlates with the phase of the stratospheric QBO. The S_q focus latitude tends to be lower and higher during the easterly and westerly phases of the stratospheric QBO, respectively. The $NINO.3$ index, which represents ENSO activity, also shows significant interannual variability (Figure 4c), but the interannual variation of the $NINO.3$ index is not coherent with the interannual variation of the S_q focus latitude. As discussed by *Liu* [2016], the stratospheric QBO has a very regular oscillation cycle around 28 months while ENSO variability consists of longer-period oscillations (∼43 and ∼62 months). A spectrum analysis of the monthly values of the S_q focus latitude anomaly revealed a peak period of ∼28 months.

Figure 4d displays the EUV measurements (0.1–50 nm) by the Solar EUV Monitor (SEM) spectrometer [*Judge et al.*, 1998] on the Solar Heliospheric Observatory (SOHO). The interannual variation of the EUV flux is dominated by the 11-year solar cycle. It is interesting to note that the period when the interannual variation of S_q focus latitude was prominent (e.g., 2005–2013) roughly corresponds to the period of low EUV flux when the year-to-year change in the EUV flux is particularly small.

The interannual variation in the geomagnetic activity index Ap is shown in Figure 4e. It is noted that the overall geomagnetic activity level is low because our analysis is limited to geomagnetically quiet days. Geomagnetic activity peaked in 2003 during the declining phase of solar cycle. However, there is no corresponding variation in the S_q focus latitude. Similar to the EUV data, the interannual variation is small during the solar minimum, when the interannual variation of the S_q focus latitude is large.

3.2. Tides in the lower thermosphere

As we showed in the previous section, the focus position of the S_q current system shows a periodic oscillation similar to the stratospheric QBO. In this section we investigate the interannual variation of atmospheric tides in the lower thermosphere, where S_q currents are driven through the ionospheric wind dynamo mechanism. Our focus is on these tidal components: $DW1$, $DE3$, and $SW2$, which are known to have large amplitudes at dynamo region heights [e.g., *Oberheide et al.*, 2011].

3.2.1. TIMED/SABER–GAIA comparisons

We first present comparisons between the temperature tides derived from TIMED/SABER data and GAIA simulation. Figures 5a and 5b compare the average seasonal variations in the amplitude of the migrating diurnal tide $DW1$ at 100 km derived from TIMED/SABER and GAIA, respectively. The model-data agreement is very good. It is known from previous studies [e.g., *Burrage et al.*, 1995; *Forbes et al.*, 2008] that the $DW1$ amplitude in the mesosphere and lower thermosphere is subject to a semiannual modulation with equinoctial maxima. Conducting numerical experiments, *McLandress* [2002a] demonstrated that the latitudinal shear in the zonal mean wind plays a role in producing seasonal variability of the migrating diurnal tide.

The interannual variation of the $DW1$ amplitude is presented in Figures 5c and 5d for TIMED/SABER and GAIA, respectively. The anomaly was computed in the same way as for the S_q focus latitude. That is, we first subtracted the average seasonal variations from the original data, and then applied the 13-month running average to the residual data. The results clearly show that the interannual variation of $DW1$ is dominated by a QBO-like oscillation. The QBO modulation of the migrating diurnal tide in the mesosphere and lower thermosphere has been reported by earlier researchers [e.g., *Hagan et al.*, 1999; *Forbes et al.*, 2008; *Wu et al.*, 2008; *Mukhtarov et al.*, 2009; *Xu et al.*, 2009]. *McLandress* [2002b] attributed the QBO modulation of $DW1$ to the change in the zonal circulation. *Mayr and Mengel* [2005] showed that the mechanism suggested by *McLandress* [2002b] is effective only below 50 km altitude, and the QBO modulation of $DW1$ above 80 km is mainly due to the momentum deposition from small-scale gravity waves.

The GAIA model reproduces the interannual variation of $DW1$ but the amplitude of the QBO oscillation is somewhat smaller compared to the TIMED/SABER observations. Figure 5e compares the stratospheric QBO at 10 hPa with the interannual variation of the $DW1$ amplitude. The results are presented for the average over 10°S–10°N where the interannual variation of $DW1$ is relatively large. It can be seen that the $DW1$ amplitude tends to be greater during the westerly phase of the stratospheric QBO. It is noted that the phase of the interannual variation of $DW1$ is shifted to later years during 2009–2014 with respect to the phase of the stratospheric QBO. The reason is unclear.

Figure 6 compares the amplitudes of the eastward-propagating non-migrating diurnal tide with wave number three, or $DE3$, at 100 km derived from TIMED/SABER and GAIA in the same format as Figure 5. The GAIA model reproduces main characteristics of seasonal and interannual variability of $DE3$. The QBO effect is evident in the amplitude anomaly (Figures 6c and 6d), consistent with previous reports [e.g., *Oberheide et al.*, 2009; *Häusler* et al., 2013]. The QBO modulation of $DE3$ weakens toward the end of the period, which can be seen in the GAIA results as well as in the TIMED/SABER data. As shown in Figure 6e, the $DE3$ amplitude tends to be greater during the westerly phase of the stratospheric QBO, similar to the $DW1$ results.

As shown in Figure 7, the model-data agreement is not as good for the semidiurnal migrating tide $SW2$. The seasonal and latitudinal patterns of $SW2$ are only in rough agreement between the TIMED/SABER measurements and GAIA simulation (Figures 7a and 7b). *Akmaev et al.* [2008] encountered a similar problem when they compared $SW2$ from TIMED/SABER with the Whole Atmosphere Model (WAM). It was considered that the difference in data sampling between observations and simulations could be a part of the reason for the disagreement. The amplitude anomaly of $SW2$ shows a complex latitudinal pattern (Figures 7c and 7d). The QBO modulation of the $SW2$ amplitude is visible in the TIMED/SABER data (Figure 7e), which is partially reproduced by GAIA. The $SW2$ amplitude tends to be greater during the easterly phase of the stratospheric QBO, when the $DW1$ and $DE3$ amplitudes become small, which is consistent with previous studies [e.g., *Forbes et al.*, 2008; *Pancheva et al.*, 2009]. The mechanism for the opposite QBO responses in $DW1$ and $SW2$ is still to be understood.

3.2.2. QBO modulation of tidal winds

Next, we examine the interannual variation of tidal winds in GAIA. The seasonal climatology was first determined for $DW1$, $DE3$, and $SW2$ in the zonal and meridional winds at 100–150 km (see Figures S1–S3 in the supporting information). Amplitude anomalies were then derived as the deviation of monthly tidal amplitudes from the seasonal climatology.

Figures 8a and 8b show the amplitude anomaly in $DW1$ at 100 km for zonal and meridional winds, respectively. The QBO effect is evident, accounting for the amplitude anomaly of up to ±3 m/s in the zonal wind and ±5 m/s in the meridional wind. Given that the GAIA model underestimates the interannual variability of $DW1$ in temperature

(Figure 5), the actual QBO effect on the tidal winds is likely to be greater. The QBO modulation of $DW1$ winds is mostly confined within $\pm 40°$ latitudes. The peak modulation occurs at ± 10–$30°$ latitudes, indicating the dominance of the (1,1) Hough mode of classical tidal theory [*Lindzen and Chapman*, 1969]. The QBO modulation of $DW1$ can also be seen at 110 km (Figures 8c and 8d) but with smaller amplitudes. At higher altitudes (Figures 8e–8h), the solar cycle effect dominates the interannual variability of $DW1$ winds. It is known that $DW1$ in the dynamo region consists of the tide from the lower atmosphere and the tide locally excited by solar EUV/UV heating [*Forbes*, 1982; *Hagan et al.*, 2001]. The strong solar cycle influence at high latitudes can be explained by the variability of $DW1$ locally generated in the thermosphere.

Figure 9 presents the results for $DE3$ winds in a similar format as Figure 8. The QBO modulation of $DE3$ is evident in the zonal wind (± 3 m/s) over the equator. The effect can be seen throughout the dynamo region. The vertical wavelength of $DE3$ is longer compared to $DW1$, which allows the wave to propagate to higher altitudes before being dissipated. Significant interannual variability can also be found in $SW2$ winds (Figure 10). However, the QBO effect is not immediately obvious, indicating that contributions by other sources are also important for $SW2$. At 150 km, the solar cycle influence dominates the interannual variability of $SW2$ winds.

3.2.3. Comparison with S_q focus latitude

We now examine the relationship between the interannual variability of the S_q focus latitude and tides. In this section, we use a bandpass filter for periods between 20 and 40 months to extract the variations around the QBO periodicity (~28 months), instead of the 13-month running mean filter used in preceding sections. The bandpass filter substantially removes the signals associated with the ENSO (>40 months) and 11-year solar cycle. Figure 11a shows the bandpass-filtered anomaly in the S_q focus latitude. As previously shown in Figure 4a, the S_q focus latitude exhibits a QBO-like variation of $\pm 2°$, most notably during 2005–2013. We first compare the results with the stratospheric QBO. Table 1 gives the correlation coefficients for the interannual variability of the S_q focus latitude over Japan and the mean zonal wind over Singapore. The bandpass filter was applied not only to the S_q focus latitude but also to the mean zonal wind. Table 1 shows that the correlation coefficient depends on height, being positive at 10 hPa ($\sim$31 km) and negative at 50 hPa ($\sim$21 km). This is because the phase of the stratospheric QBO varies with height (see Figure 4b). The strongest correlation was obtained at 20 hPa ($\sim$26 km) where the variations in the S_q focus latitude and mean zonal wind are in phase. The correlation coefficient is as high as 0.93 when the analysis is limited to the period 2005–2013.

Figure 11b shows the bandpass-filtered anomaly in the $DW1$ meridional wind amplitude at 18°N. Different colors correspond to different altitudes. The QBO influence is apparent at 100 and 110 km. These tidal variations are nearly in phase with the variation in the S_q focus latitude, which is reflected in the high correlation coefficients: 0.91 at 100 km and 0.90 at 110 km during 2005–2013 (see Table 1).

Figure 11c is the same as Figure 11b but for the $DE3$ zonal wind amplitude at 4°N. The QBO modulation of the $DE3$ wind is visible at all heights without any phase shift. A comparison with the S_q focus latitude reveals high correlation coefficients throughout the dynamo region (Table 1). Figure 11d shows the bandpass-filtered anomaly in the $SW2$ meridional wind at 57°N, where the interannual variability of the tide is most pronounced (see Figure 10). The tidal variations are not well correlated with the S_q focus latitude (Table 1) nor with the stratospheric QBO. Thus, the interannual variability of $SW2$ winds may be dominated by other sources than QBO.

4. Discussion

The speculation about the stratospheric QBO influence on the ionospheric wind dynamo has existed for many years without compelling evidence. Some studies found a weak geomagnetic variation at a period around 27 months [*Stacey and Wescott*, 1962; *Yacob and Bhargava*, 1968; *Olsen*, 1994; *Jarvis*, 1996, 1997], while other studies did not find such a peak in the geomagnetic spectrum [*London and Matsushita*, 1963; *Shapiro and Ward*, 1964; *Love and Rigler*, 2014]. It has often been a matter of debate whether the quasi two year oscillation in the geomagnetic field is associated with the stratospheric QBO or the same period of oscillation in solar activity [e.g., *Yacob and Bhargava*, 1968; *Sugiura and Poros*, 1977]. In the latter case, the geomagnetic variation arises from changes in ionospheric conductivities rather than neutral winds. We showed that the QBO-like variation in the S_q current system is evident during the solar minimum period when interannual variability of solar activity is small. Besides, the latitudinal position of the S_q current focus is not sensitive to solar activity (see Figure 3). Based on these observations, we can rule out the possibility of the dominant solar contribution to the interannual variation of the S_q focus latitude.

The S_q current system can be regarded as a superposition of the current systems driven by different tides. Since different tides drive different patterns of the ionospheric current system, changes in the tidal composition would affect the shape and intensity of the S_q current system [e.g., *Richmond et al.*, 1976; *Stening*, 1989; *Yamazaki et al.*, 2012b].

Using the GAIA model as well as TIMED/SABER measurements, we showed that the atmospheric tides $DW1$, $DE3$, and $SW2$ in the dynamo region are significantly influenced by the stratospheric QBO, supplementing previous observations and numerical results [e.g., *Forbes et al.*, 2008; *Liu*, 2014]. We made direct comparisons between the interannual variations in the tidal wind amplitudes and the S_q focus latitude, finding that the QBO-like variation of the S_q current focus is highly correlated with the interannual variations in the diurnal tidal amplitudes (i.e., $DW1$ and $DE3$) in the dynamo region. These results suggest that the quasi two year variation of the S_q current system is likely due to tidal variability associated with the stratospheric QBO.

It is beyond the scope of the present study to determine the relative contribution of different tides ($DW1$, $DE3$, $SW2$, and other tides) to the QBO modulation of S_q. Further numerical experiments would be necessary to clarify which tide plays a dominant role in the QBO modulation of the ionospheric wind dynamo and how exactly the tide affects the latitudinal position of the S_q current focus. Although the $SW2$ wind amplitude in GAIA did not clearly show the QBO influence, the possible contribution of $SW2$ cannot be excluded because of the limited ability of GAIA in reproducing the interannual variability of $SW2$ (see Figure 7).

More efforts are required to establish the morphology of the QBO effect on the ionospheric dynamo. Observations in different longitudes could provide insights into the role of non-migrating tides. Also, it needs to be clarified whether the QBO effect on the S_q focus latitude can be observed in the Southern Hemisphere.

Our results showed no obvious correlation between the interannual variations of the ENSO activity index and S_q focus latitude (Figure 4). However, it is possible that the

ENSO activity affects the S_q current system indirectly by modulating the stratospheric QBO. Studies have shown that the amplitude and phase of the stratospheric QBO depend on ENSO activity [*Taguchi*, 2010; *Yuan et al.*, 2014; *Geller et al.*, 2016]. The possible ENSO effect on the ionospheric wind dynamo should be further investigated.

The interannual variation of the S_q focus latitude over Japan was most evident during 2005–2013, when the solar EUV flux was low. It is possible that the QBO modulation of the ionospheric dynamo is solar cycle dependent. A longer data set would be necessary to clarify the impact of solar activity. An important piece of information obtained from the GAIA simulation is that the QBO modulation of tidal winds occurred in the dynamo region throughout the period examined, regardless of solar activity. Thus, the apparent absence of the QBO signal during 1999–2004 is not due to the absence of the QBO variation in tides, but due to other mechanisms that make the QBO modulation of the S_q current system undetectable. The numerical study by *Liu and Richmond* [2013] showed that the meteorological contribution to ionospheric variability is more significant in solar minimum conditions than in solar maximum conditions. During solar maximum, the ionospheric dynamo at F-region heights (above 150 km) becomes important, thus the contribution by the E-region dynamo, which is more responsive to meteorological forcing, is relatively small. More discussion on the role of the F-region dynamo in the S_q current system and its solar activity dependence can be found in *Maute and Richmond* [2016].

A natural question that arises from the present study is whether the QBO modulation of the ionospheric wind dynamo has a broader impact on the ionosphere. A number of studies have already reported on the quasi two year variation in the ionospheric plasma density [*Chen*, 1992; *Kane*, 1995; *Echer*, 2007; *Tang et al.*, 2014; *Zhou et al.*, 2016; *Chang* *et al.*, 2016], but the association with the stratospheric QBO is yet to be established. *Yamazaki and Richmond* [2013] numerically showed that there are two mechanisms by which upward-propagating tides in the lower thermosphere can affect the ionosphere. One is through the electrodynamic effect. That is, the electric field generated by the dynamo action of tides will modulate the plasma transport perpendicular to the geomagnetic field, which is dominated by the so-called $\mathbf{E}\times\mathbf{B}$ drift. The other mechanism is tidal mixing. The dissipation of tidal waves alters the mean circulation of the thermosphere, which in turn modulates the thermospheric composition that determines the production and loss rates of the ionospheric plasma (see also *Jones et al.* [2014a,b] for detailed discussions on the tidal mixing mechanism). *Chang et al.* [2016] showed observational evidence that tidal mixing, along with the direct solar effect, is in play in the ionospheric QBO. More numerical work is required to determine the relative importance of different mechanisms for the ionospheric QBO.

5. Conclusions

The main results of the present study may be summarized as follows:

1. The latitude of the S_q current focus, estimated using a dense magnetometer network over Japan for 1999–2015, shows an interannual variation of $\pm 2°$.

2. A quasi two year variation is found in the S_q focus latitude during 2005–2013. The S_q focus latitude tends to be higher and lower during the westerly and easterly phases of the stratospheric QBO, respectively.

3. No corresponding interannual variation is found in the ENSO activity index $NINO.3$, solar EUV flux, or geomagnetic activity index Ap.

4. The QBO-like variation of the S_q focus latitude is highly correlated with the amplitude variations of $DW1$ and $DE3$ tidal winds in the dynamo region.

These results suggest that the variation of atmospheric tides due to the stratospheric QBO could be an importance source for interannual variability of the ionospheric wind dynamo.

Acknowledgments.

Geomagnetic data for Memambetsu, Kakioka, and Kanoya were provided by the Japan Meteorological Agency and available at the website of the Kakioka Magnetic Observatory at http://www.kakioka-jma.go.jp/en/. The other geomagnetic data were provided by the Geospatial Information Authority of Japan and available at http://www.gsi.go.jp/buturisokuchi/geomag_index.html (Japanese). We thank both the institutions for their commitment to the long-term operation. The disturbance storm time index *Dst* was provided by the World Data Center for geomagnetism, Kyoto (http://wdc.kugi.kyoto-u.ac.jp/dstdir/). The list of geomagnetically quietest days of each month and the geomagnetic activity index *Ap* were provided by the GFZ German Research Centre for Geosciences, available at http://www.gfz-potsdam.de/kp-index. The SABER temperature data were downloaded from http://saber.gats-inc.com/index.php. We thank the SABER science team and Gats Inc. for processing and distributing the SABER data. GAIA simulation was performed using the computer systems at National Institute of Information and Communications Technology, Japan. The meteorological reanalysis data used in the GAIA simulation were provided from the cooperative research project of the JRA-25 long-term reanalysis by the Japan Meteorological Agency and the Central Research Institute of Electric Power Industry. The GAIA model data presented in this paper will be made available upon request. The radiosonde data for the monthly mean zonal wind at Singapore were downloaded from the website of Freie Universität Berlin (FUB) at http://www.geo.fu-berlin.de/en/met/ag/strat/produkte/qbo/. The ENSO activity index $NINO.3$ was provided by the Japan Meteorological Agency, available at http://www.data.jma.go.jp/gmd/cpd/db/elnino/index/dattab.html (Japanese).

The SOHO/SEM EUV data were obtained from the website of Space Science Center, University of Southern California at `http://www.usc.edu/dept/space_science/sem_data/sem_data.html`. Y.Y. and M.J.K. was supported by Natural Environment Research Council grant NE/K01207X/1. H.L. aknowledges support by JSPS KAKENHI grant 15K05301, 15H02135. Y.-Y.S. was supported by the NICT International Exchange Program. Y.M. acknowledges supported by JSPS KAKENHI grant (B)15H03733.

References

Akmaev, R. A., T. J. Fuller-Rowell, F. Wu, J. M. Forbes, X. Zhang, A. F. Anghel, M. D. Iredell, S. Moorthi, and H.-M. Juang (2008), Tidal variability in the lower thermosphere: Comparison of Whole Atmosphere Model (WAM) simulations with observations from TIMED, *Geophys. Res. Lett.*, *35*, L03810, doi:10.1029/2007GL032584.

Burrage, M. D., M. E. Hagan, W. R. Skinner, D. L. Wu, and P. B. Hays (1995), Long-term variability in the solar diurnal tide observed by HRDI and simulated by the GSWM, *Geophys. Res. Lett.*, *22*, 2641–2644.

Chang, L. C., Y.-Y. Sun, J. Yue, J. C. Wang, and S.-H. Chien (2016), Coherent seasonal, annual, and quasi-biennial variations in ionospheric tidal/SPW amplitudes, *J. Geophys. Res. Space Physics*, *121*, 6970–6985, doi:10.1002/2015JA022249.

Chen, P.-R. (1992), Evidence of the ionospheric response to the QBO, *Geophys. Res. Lett.*, *19*, 1089–1092.

Chulliat, A., P. Vigneron, G. Hulot (2016), First results from the Swarm dedicated ionospheric field inversion chain, *Earth Planets Space*, *68*(104), doi:10.1186/s40623-016-0481-6.

Echer, E. (2007), On the quasi-biennial oscillation (QBO) signal in the foF2 ionospheric parameter, *J. Atmos. Sol. Terr. Phys.*, *69*, 621–627.

Forbes, J. M. (1982), Atmospheric tides: 1. Model description and results for the solar diurnal component, *J. Geophys. Res.*, *87*(A7), 5222–5240, doi:10.1029/JA087iA07p05222.

Forbes, J. M., X. Zhang, S. Palo, J. Russell, C. J. Mertens, and M. Mlynczak (2008), Tidal variability in the ionospheric dynamo region, *J. Geophys. Res.*, *113*, A02310, doi:10.1029/2007JA012737.

Gan Q., J. Du, W. E. Ward, S. R. Beagley, V. I Fomichev, S. Zhang (2014) Climatology of the diurnal tides from eCMAM30 (1979 to 2010) and its comparisons with SABER, *Earth Planets Space*, *66*(103), doi:10.1186/1880-5981-66-103.

Geller, M. A., T. Zhou, and W. Yuan (2016), The QBO, gravity waves forced by tropical convection, and ENSO, *J. Geophys. Res. Atmos.*, *121*, 8886–8895, doi:10.1002/2015JD024125.

Hagan, M. E., M. D. Burrage, J. M. Forbes, J. Hackney, W. J. Randel, and X. Zhang (1999), QBO effects on the diurnal tide in the upper atmosphere, *Earth Planets Space*, *51*, 571–578.

Hagan, M. E., R. G. Roble, and J. Hackney (2001), Migrating thermospheric tides, *J. Geophys. Res.*, *106*(A7), 12739–12752, doi:10.1029/2000JA000344.

Häusler, K., J. Oberheide, H. Lühr, and R. Koppmann (2013), The geospace response to nonmigrating tides, in *Climate and Weather of the Sun-Earth System (CAWSES): Highlights from a Priority Program*, edited by F.-J. Lübken, 481–506, Springer Atmospheric Sciences, Dordrecht, Heidelberg, New York, London, doi:10.1007/978-94-007-4348-9.

Jarvis, M. J. (1996), Quasi-biennial oscillation effects in the semidiurnal tide of the Antarctic lower thermosphere, *Geophys. Res. Lett.*, *23*, 2661–2664. doi:10.1029/96GL02394.

Jarvis, M. J. (1997), Latitudinal variation of quasi-biennial oscillation modulation of the semidiurnal tide in the lower thermosphere, *J. Geophys. Res.*, *102*(A12), 27177–27187, doi:10.1029/97JA02034.

Jin, H., Y. Miyoshi, H. Fujiwara, H. Shinagawa, K. Terada, N. Terada, M. Ishii, Y. Otsuka, and A. Saito (2011), Vertical connection from the tropospheric activities to the ionospheric longitudinal structure simulated by a new Earths whole atmosphere-ionosphere coupled model, *J. Geophys. Res.*, *116*, A01316, doi:10.1029/2010JA015925.

Jin, H., Y. Miyoshi, D. Pancheva, P. Mukhtarov, H. Fujiwara, and H. Shinagawa (2012), Response of migrating tides to the stratospheric sudden warming in 2009 and their effects on the ionosphere studied by a whole atmosphere-ionosphere model GAIA with COSMIC and TIMED/SABER observations, *J. Geophys. Res.*, *117*, A10323, doi:10.1029/2012JA017650.

Jones, M., Jr., J. M. Forbes, M. E. Hagan, and A. Maute (2014a), Impacts of vertically propagating tides on the mean state of the ionosphere-thermosphere system, *J. Geophys. Res. Space Physics*, *119*, 2197–2213, doi:10.1002/2013JA019744.

Jones, M., Jr., J. M. Forbes, and M. E. Hagan (2014), Tidal-induced net transport effects on the oxygen distribution in the thermosphere, *Geophys. Res. Lett.*, *41*, 5272–5279, doi:10.1002/2014GL060698.

Judge, D. L., et al. (1998), First solar EUV irradiances obtained from SOHO by the CELIAS/SEM, *Solar Phys.*, *177*, 161–173.

Kane, R. P. (1995), Quasi-biennial oscillation in ionospheric parameters measured at Juliusruh (55°N, 13°E), *J. Atmos. Terr. Phys.*, *57*, 415–419.

Kawano-Sasaki, K., and S. Miyahara (2008), A study on three-dimensional structures of the ionospheric dynamo currents induced by the neutral winds simulated by the Kyushu-GCM, *J. Atmos. Sol. Terr. Phys.*, *70*, 1549–1562.

Lindzen, R. S., and S. Chapman (1969), Atmospheric tides, *Space Sci. Rev.*, *10*, 3–188.

Liu, H. (2016), Thermospheric inter-annual variability and its potential connection to ENSO and stratospheric QBO, *Earth, Planets and Space*, *68*(77), doi:10.1186/s40623-016-0455-8.

Liu, H., H. Jin, Y. Miyoshi, H. Fujiwara, and H. Shinagawa (2013), Upper atmosphere response to stratosphere sudden warming: Local time and height dependence simulated by GAIA model, *Geophys. Res. Lett.*, *40*, 635–640, doi:10.1002/grl.50146.

Liu, H.-L. (2014), WACCM-X simulation of tidal and planetary wave variability in the upper atmosphere, in *Modeling the Ionosphere-Thermosphere System*, edited by J. Huba, R. Schunk, and G. Khazanov, John Wiley, Chichester, U.K., doi:10.1002/9781118704417.ch16.

Liu, H.-L., and A. D. Richmond (2013), Attribution of ionospheric vertical plasma drift perturbations to large-scale waves and the dependence on solar activity, *J. Geophys. Res. Space Physics*, *118*, 2452–2465, doi:10.1002/jgra.50265.

London, J., and S. Matsushita (1963), Periodicities of the geomagnetic variation field at Huancayo, Peru, *Nature*, *198*, 374.

Love, J., and E. J. Rigler (2014), The magnetic tides of Honolulu, *Geophys. J. Int.*, *197*, 1335–1353, doi:10.1093/gji/ggu090.

Maute, A., and A. D. Richmond (2016), F-region dynamo simulations at low and mid-Latitude, *Space Sci. Rev.*, 1–23, doi:10.1007/s11214-016-0262-3.

Mayr, H. G., and J. G. Mengel (2005), Interannual variations of the diurnal tide in the mesosphere generated by the quasi-biennial oscillation, *J. Geophys. Res.*, *110*, D10111, doi:10.1029/2004JD005055.

McLandress, C. (2002a), The seasonal variation of the propagating diurnal tide in the mesosphere and lower thermosphere. Part II: The role of tidal heating and zonal mean zonal winds, *J. Atmos. Sci.*, *59*, 907–921.

McLandress, C. (2002b), Interannual variations of the diurnal tide in the mesosphere induced by a zonal-mean wind oscillation in the tropics, *Geophys. Res. Lett.*, *29*(9), doi:10.1029/2001GL014551.

Miyoshi, Y., H. Fujiwara, H. Jin, H. Shinagawa, and H. Liu (2012), Numerical simulation of the equatorial wind jet in the thermosphere, *J. Geophys. Res.*, *117*, A03309, doi:10.1029/2011JA017373.

Mukhtarov, P., D. Pancheva, and B. Andonov (2009), Global structure and seasonal and interannual variability of the migrating diurnal tide seen in the SABER/TIMED temperatures between 20 and 120 km, *J. Geophys. Res.*, *114*, A02309, doi:10.1029/2008JA013759.

Naujokat, B. (1986), An update of the observed quasi-biennial oscillation of the stratospheric winds over the tropics, *J. Atmos. Sci.*, *43*, 1873–1877.

Oberheide, J., J. M. Forbes, K. Häusler, Q. Wu, and S. L. Bruinsma (2009), Tropospheric tides from 80 to 400 km: Propagation, interannual variability, and solar cycle effects, *J. Geophys. Res.*, *114*, D00I05, doi:10.1029/2009JD012388.

Oberheide, J., J. M. Forbes, X. Zhang, and S. L. Bruinsma (2011), Climatology of upward propagating diurnal and semidiurnal tides in the thermosphere, *J. Geophys. Res.*, *116*, A11306, doi:10.1029/2011JA016784.

Olsen, N. (1994), A 27-month periodicity in the low latitude geomagnetic field and its connection to the stratospheric QBO, *Geophys. Res. Lett.*, *21*, 1125–1128, doi:10.1029/94GL00180.

Onogi, K. et al., (2007), The JRA-25 Reanalysis. *J. Meteor. Soc. Japan*, *85*, 369–432, doi:10.2151/jmsj.85.369.

Pancheva, D., P. Mukhtarov, and B. Andonov (2009) Global structure, seasonal and interannual variability of the migrating semidiurnal tide seen in the SABER/TIMED temperatures (2002–2007), *Ann. Geophys.*, *27*,687–703.

Pedatella, N. M., and H.-L. Liu (2012), Tidal variability in the mesosphere and lower thermosphere due to the El Niño–Southern Oscillation, *Geophys. Res. Lett.*, *39*, L19802, doi:10.1029/2012GL053383.

Pedatella, N. M., and H.-L. Liu (2013), Influence of the El Niño Southern Oscillation on the middle and upper atmosphere, *J. Geophys. Res. Space Physics*, *118*, 2744–2755, doi:10.1002/jgra.50286.

Remsberg, E. E., et al. (2008), Assessment of the quality of the Version 1.07 temperature-versus-pressure profiles of the middle atmosphere from TIMED/SABER, *J. Geophys. Res.*, *113*, D17101, doi:10.1029/2008JD010013.

Richmond, A. D., S. Matsushita, and J. D. Tarpley (1976), On the production mechanism of electric currents and fields in the ionosphere, *J. Geophys. Res.*, *81*(4), 547–555, doi:10.1029/JA081i004p00547.

Shapiro, R., and F. Ward (1964), Possibility of a 26- or 27-month periodicity in the equatorial geomagnetic field, *Nature*, *201*, 909.

Stacey, F. D., and P. Wescott (1962), Possibility of a 26- or 27-month periodicity in the equatorial geomagnetic field and its correlation with stratospheric winds, *Nature*, *196*, 730–732.

Stening, R. J. (1989), A calculation of ionospheric currents due to semidiurnal antisymmetric tides, *J. Geophys. Res.*, *94*(A2), 1525–1531, doi:10.1029/JA094iA02p01525.

Stening, R., T. Reztsova, D. Ivers, J. Turner, and D. Winch (2005), A critique of methods of determining the position of the focus of the Sq current system, *J. Geophys. Res.*, *110*, A04305, doi:10.1029/2004JA010784.

Stening, R., T. Reztsova, and L. H. Minh (2007), Variation of Sq focus latitudes in the Australian/Pacific region during a quiet sun year, *J. Atmos. Sol. Terr. Phys.*, *69*, 734–740.

Sugiura, M., and D. J. Poros (1977), Solar-generated quasi-biennial geomagnetic variation, *J. Geophys. Res.*, *82*(35), 5621–5628, doi:10.1029/JA082i035p05621.

Taguchi, M. (2010), Observed connection of the stratospheric quasi-biennial oscillation with El Niño–Southern Oscillation in radiosonde data, *J. Geophys. Res.*, *115*, D18120, doi:10.1029/2010JD014325.

Takeda, M. (1990), Geomagnetic field variation and the equivalent current system generated by an ionospheric dynamo at the solstice, *J. Atmos. Terr. Phys.*, *52*, 59–67.

Takeda, M. (1999), Time variation of global geomagnetic Sq field in 1964 and 1980, *J. Atmos. Sol. Terr. Phys.*, *61*, 765–774.

Takeda, M. (2002), Features of global geomagnetic Sq field from 1980 to 1990, *J. Geophys. Res.*, *107*(A9), 1252, doi:10.1029/2001JA009210.

Takeda, M. (2013), Contribution of wind, conductivity, and geomagnetic main field to the variation in the geomagnetic Sq field, *J. Geophys. Res. Space Physics*, *118*, 4516–4522, doi:10.1002/jgra.50386.

Tang, W., X.-H. Xue, J. Lei, and X.-K. Dou (2014), Ionospheric quasi-biennial oscillation in global TEC observations, *J. Atmos. Sol. Terr. Phys.*, *107*, 36–41.

Vichare, G., R. Rawat, M. Jadhav, A. K. Sinha (2016), Seasonal variation of the Sq focus position during 2006–2010, *Adv. Space Res.*, http://dx.doi.org/10.1016/j.asr.2016.10.009.

Wu, Q., D. A. Ortland, T. L. Killeen, R. G. Roble, M. E. Hagan, H.-L. Liu, S. C. Solomon, J. Xu, W. R. Skinner, and R. J. Niciejewski (2008), Global distribution and interannual variations of mesospheric and lower thermospheric neutral wind diurnal tide: 1. Migrating tide, *J. Geophys. Res.*, *113*, A05308, doi:10.1029/2007JA012542.

Xu, J., A. K. Smith, H.-L. Liu, W. Yuan, Q. Wu, G. Jiang, M. G. Mlynczak, J. M. Russell III, and S. J. Franke (2009), Seasonal and quasi-biennial variations in the migrating diurnal tide observed by Thermosphere, Ionosphere, Mesosphere, Energetics and Dynamics (TIMED), *J. Geophys. Res.*, *114*, D13107, doi:10.1029/2008JD011298.

Yacob, A., and B. N. Bhargava (1968), On 26-month periodicity in quiet-day range of geomagnetic horizontal force and in sunspot number, *J. Atmos. Terr. Phys.*, *30*, 1907–1911.

Yamazaki, Y., and A. D. Richmond (2013), A theory of ionospheric response to upward-propagating tides: Electrodynamic effects and tidal mixing effects, *J. Geophys. Res.*

Space Physics, *118*, 5891–5905, doi:10.1002/jgra.50487.

Yamazaki, Y., and A. Maute (2016), Sq and EEJ–A review on the daily variation of the geomagnetic field caused by ionospheric dynamo currents, *Space Sci. Rev.*, 1–107, doi:10.1007/s11214-016-0282-z.

Yamazaki, Y., et al. (2011), An empirical model of the quiet daily geomagnetic field variation, *J. Geophys. Res.*, *116*, A10312, doi:10.1029/ 2011JA016487.

Yamazaki, Y., K. Yumoto, D. McNamara, T. Hirooka, T. Uozumi, K. Kitamura, S. Abe, and A. Ikeda (2012a), Ionospheric current system during sudden stratospheric warming events, *J. Geophys. Res.*, *117*, A03334, doi:10.1029/2011JA017453.

Yamazaki, Y., A. D. Richmond, H. Liu, K. Yumoto, and Y. Tanaka (2012b), Sq current system during stratospheric sudden warming events in 2006 and 2009, *J. Geophys. Res.*, *117*, A12313, doi:10.1029/2012JA018116.

Yamazaki, Y., K. Häusler, and J. A. Wild (2016), Day-to-day variability of midlatitude ionospheric currents due to magnetospheric and lower atmospheric forcing, *J. Geophys. Res. Space Physics*, *121*, doi:10.1002/2016JA022817.

Yuan, W., M. A. Geller, and P. T. Love (2014), ENSO influence on QBO modulations of the tropical tropopause, *Q. J. R. Meteorol. Soc.*, *140*, 1670–1676, doi:10.1002/qj.2247.

Zhou, Y.-L., Li, Wang, C. Xiong, H. Lühr, S.-Y. Ma (2016), The solar activity dependence of nonmigrating tides in electron density at low and middle latitudes observed by CHAMP and GRACE, *Ann. Geophys.*, *34*, 463–472.

Table 1. Correlation coefficients for the interannual variations of the S_q focus latitude and other parameters. It is noted that the 20–40 month bandpass filter was applied to all the variables before calculating the correlation coefficients.

	S_q focus latitude anomaly (1999–2015)	S_q focus latitude anomaly (2005–2013)
Mean zonal wind		
10 hPa, ∼31 km	0.53	0.57
20 hPa, ∼26 km	0.82	0.93
50 hPa, ∼21 km	-0.33	-0.31
$DW1$ amplitude anomaly (meridional wind at 18°N)		
100 km	0.79	0.91
110 km	0.78	0.90
130 km	0.53	0.60
150 km	0.28	0.19
$DE3$ amplitude anomaly (zonal wind at 4°N)		
100 km	0.80	0.96
110 km	0.78	0.93
130 km	0.81	0.93
150 km	0.81	0.93
$SW2$ amplitude anomaly (meridional wind at 57°N)		
100 km	0.21	0.41
110 km	-0.04	-0.05
130 km	-0.08	-0.18
150 km	-0.29	-0.31

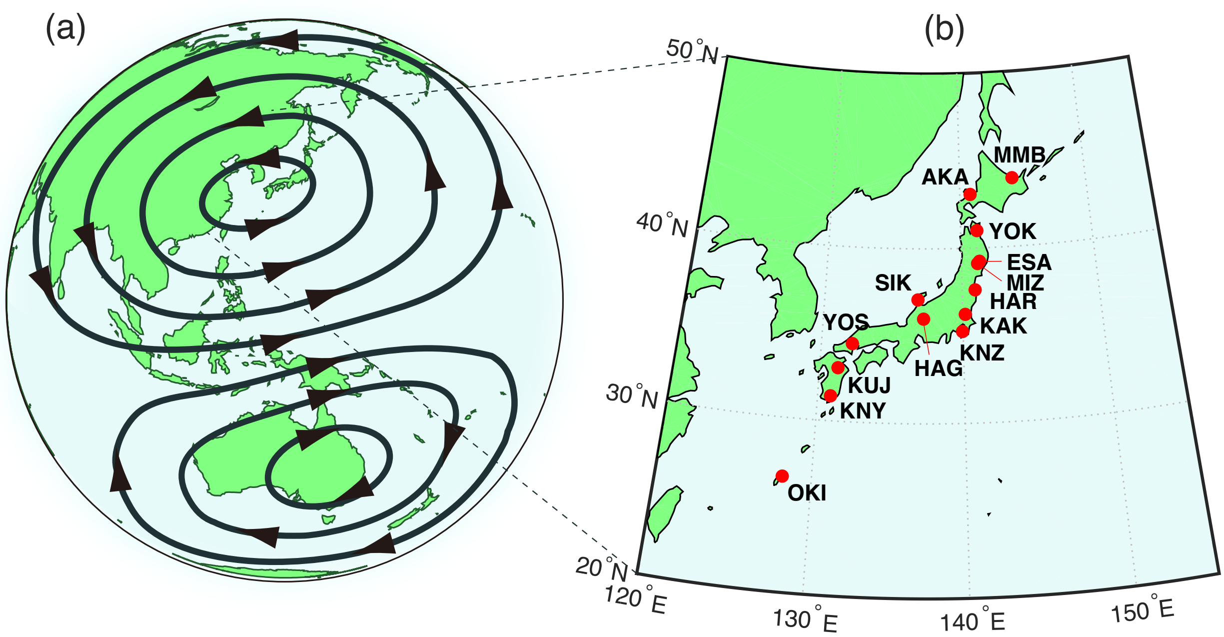

Figure 1. (a) Schematic illustrating the dayside pattern of the S_q current system. Note that the center of the S_q current loop in the Northern Hemisphere usually appears over Japan. (b) A map of the geomagnetic observatories used in this study. The following are the name and coordinates of each observatory: Memambetsu (MMB, 43.9°N, 144.2°E), Akaigawa (AKA, 43.1°N, 140.8°E), Yokohama (YOK, 41.0°N, 141.2°E), Esashi (ESA, 39.2°, 141.4°E), Mizusawa (MIZ, 39.1°N, 141.2°E), Haramachi (HAR, 37.6°N, 141.0°E), Shika (SIK, 37.1°N, 136.8°E), Kakioka (KAK, 36.2°N, 140.2°E), Hagiwara (HAG, 36.0°N, 137.2°), Kanozan (KNZ, 35.2°, 140.0°E), Yoshiwa (YOS, 34.5°N, 132.2°E), Kuju (KUJ, 33.1°N, 131.3°E), Kanoya (KNY, 31.4°N, 130.9°E), Okinawa (OKI, 26.6°N, 128.1°E).

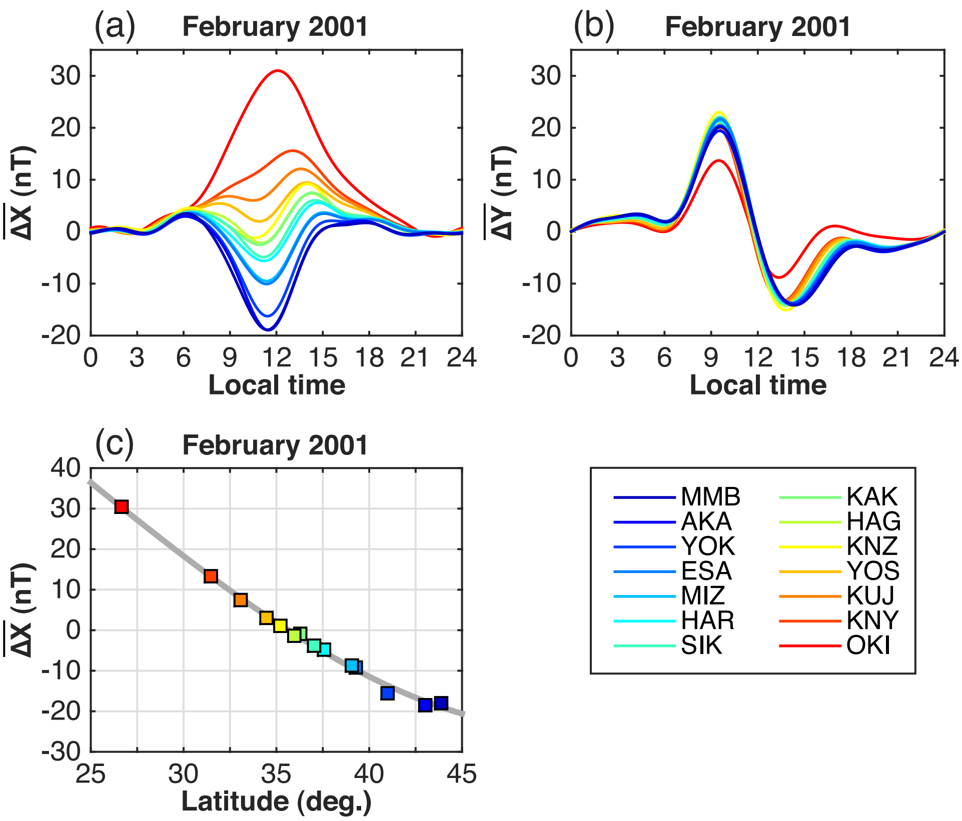

Figure 2. (a,b) Average quiet-day geomagnetic daily variations $\overline{\Delta X}$ and $\overline{\Delta Y}$ for February 2001. Different colors represent different observatories. (c) A scatter plot of $\overline{\Delta X}$ at the time of $\overline{\Delta Y}$=0 as a function of latitude.

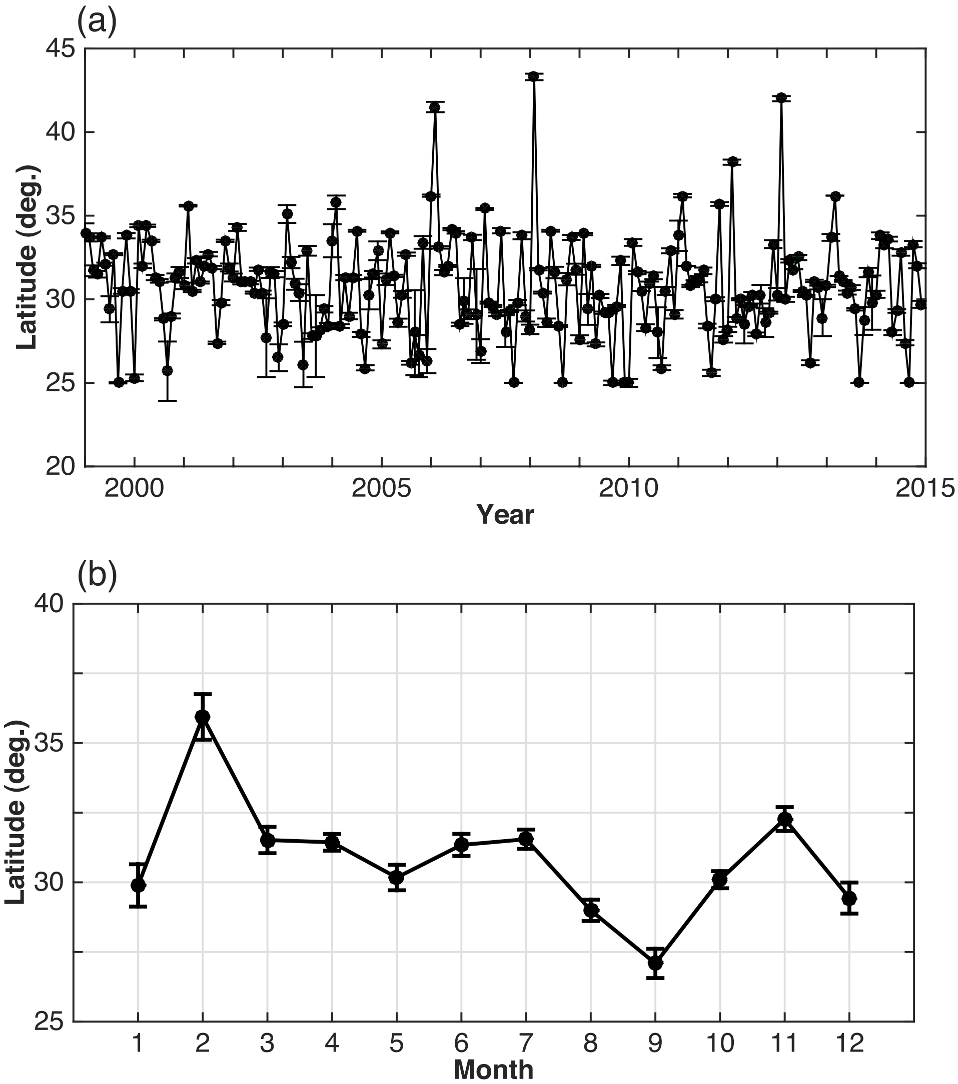

Figure 3. The latitude of the northern S_q current focus over Japan. (a) Monthly values from January 1999 to December 2015. The error bars have a length of twice the 1-σ error estimated by a Monte Carlo simulation. (b) The average seasonal variation during 1999–2015. The error bars represent the standard error of the mean.

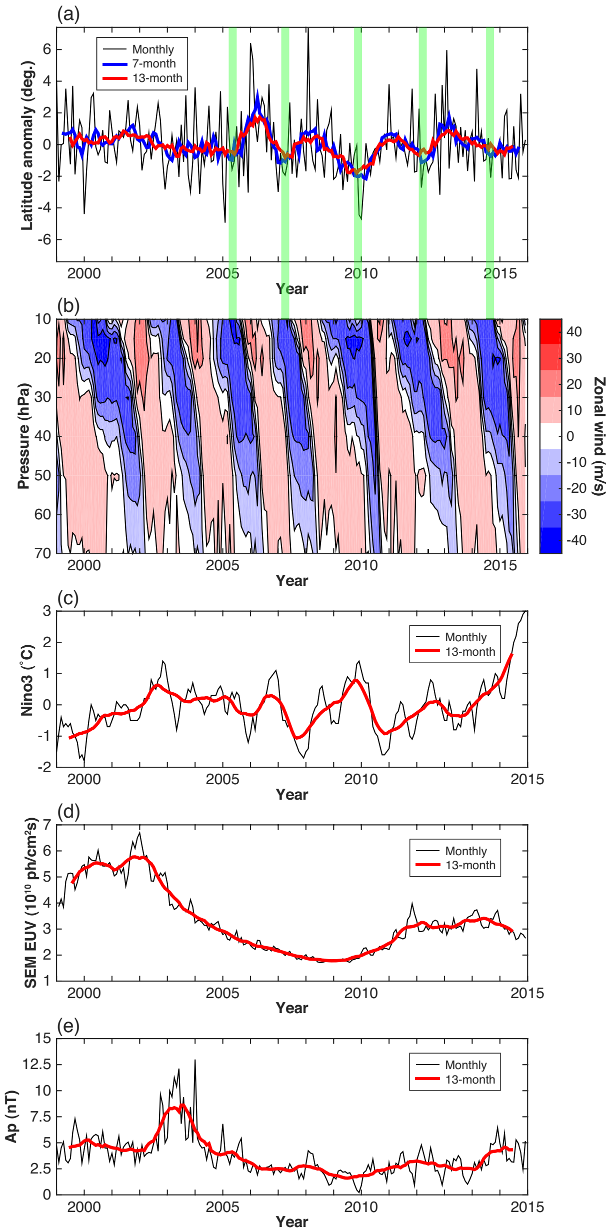

Figure 4. (a) The anomaly in the S_q focus latitude during 1999–2015. (b) The monthly mean zonal wind over Singapore. The pressure levels 70 hPa and 10 hPa roughly correspond to the altitudes 18 km and 31 km, respectively. The periodic change in the wind direction represents the stratospheric QBO. (c) The ENSO activity index $NINO.3$. The periods when the $NINO.3$ index shows large positive and negative deviations correspond to El Niño and La Niña, respectively. (d) The solar EUV flux (0.1–50 nm) from SOHO/SEM. (e) The geomagnetic activity index Ap. For (a), (d) and (e), the monthly values are calculated using only the data corresponding to the ten quietest days of each month.

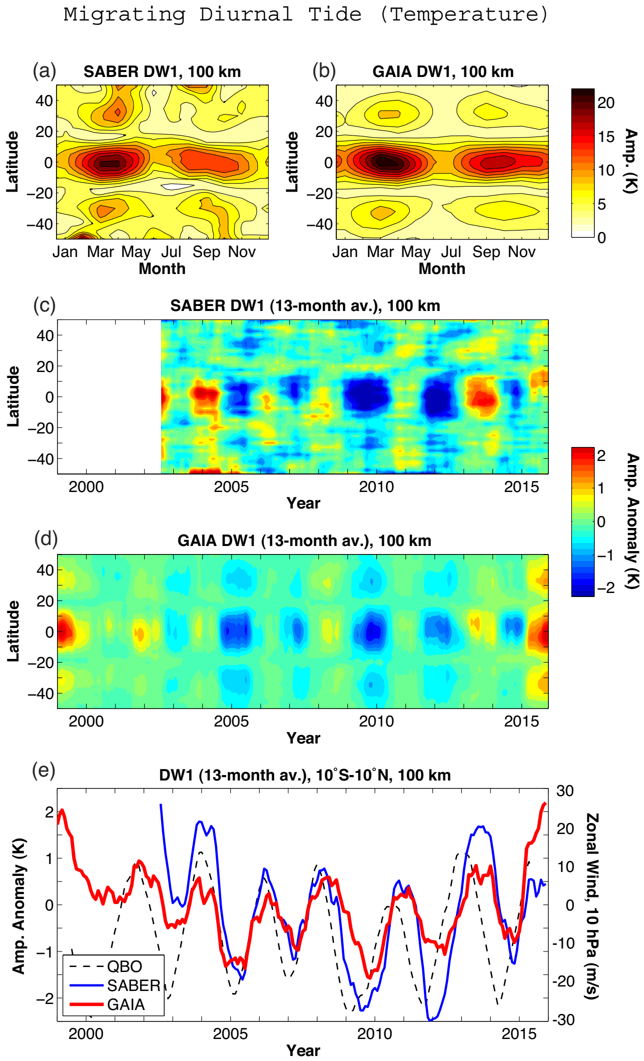

Figure 5. The amplitude of the migrating diurnal tide $DW1$ at 100 km. (a,b) The average seasonal variations for 1999–2015 derived from TIMED/SABER data and GAIA model. (c,d) The tidal amplitude anomaly, smoothed by a 13-month running mean. (e) A comparison between the interannual variation of the tide at 10°S–10°N latitudes (solid lines, left axis) and stratospheric QBO (dashed line, right axis).

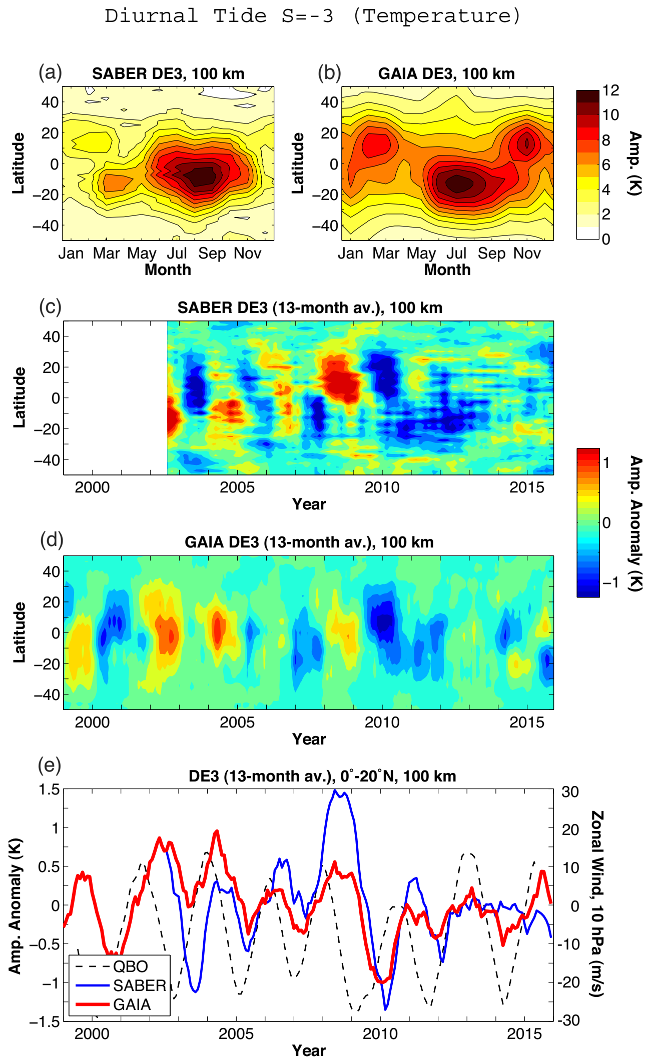

Figure 6. The amplitude of the eastward-propagating non-migrating diurnal tide with wavenumber three $DE3$ at 100 km. (a,b) The average seasonal variations for 1999–2015 derived from TIMED/SABER data and GAIA model. (c,d) The tidal amplitude anomaly, smoothed by a 13-month running mean. (e) A comparison between the interannual variation of the tide at 0°–20°N latitudes (solid lines, left axis) and stratospheric QBO (dashed line, right axis).

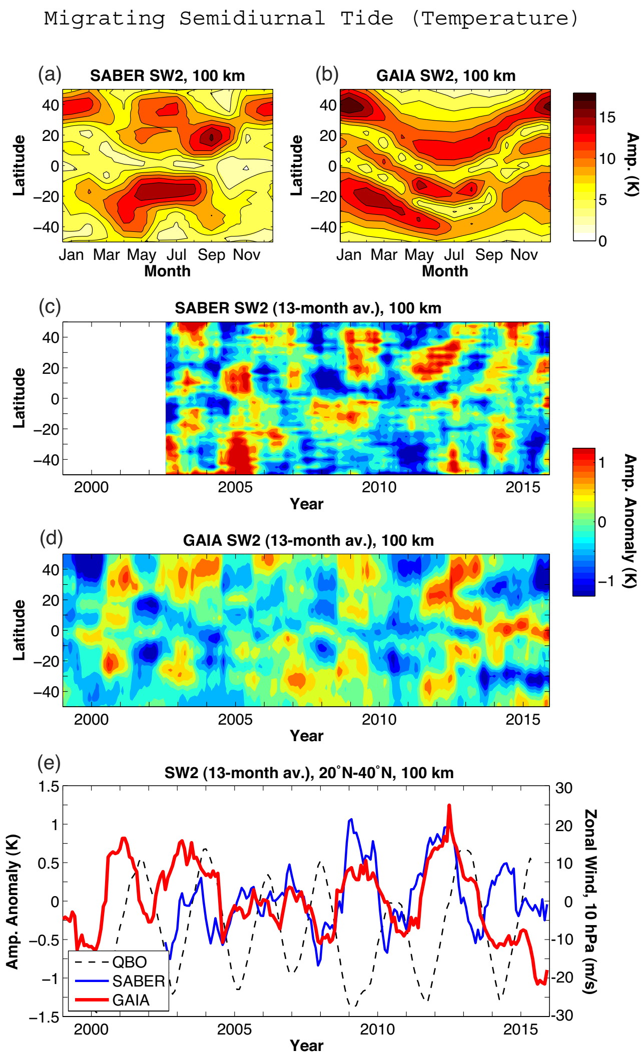

Figure 7. The amplitude of the migrating semidiurnal tide $SW2$ at 100 km. (a,b) The average seasonal variations for 1999–2015 derived from TIMED/SABER data and GAIA model. (c,d) The tidal amplitude anomaly, smoothed by a 13-month running mean. (e) A comparison between the interannual variation of the tide at 10°N–30°N latitudes (solid lines, left axis) and stratospheric QBO (dashed line, right axis).

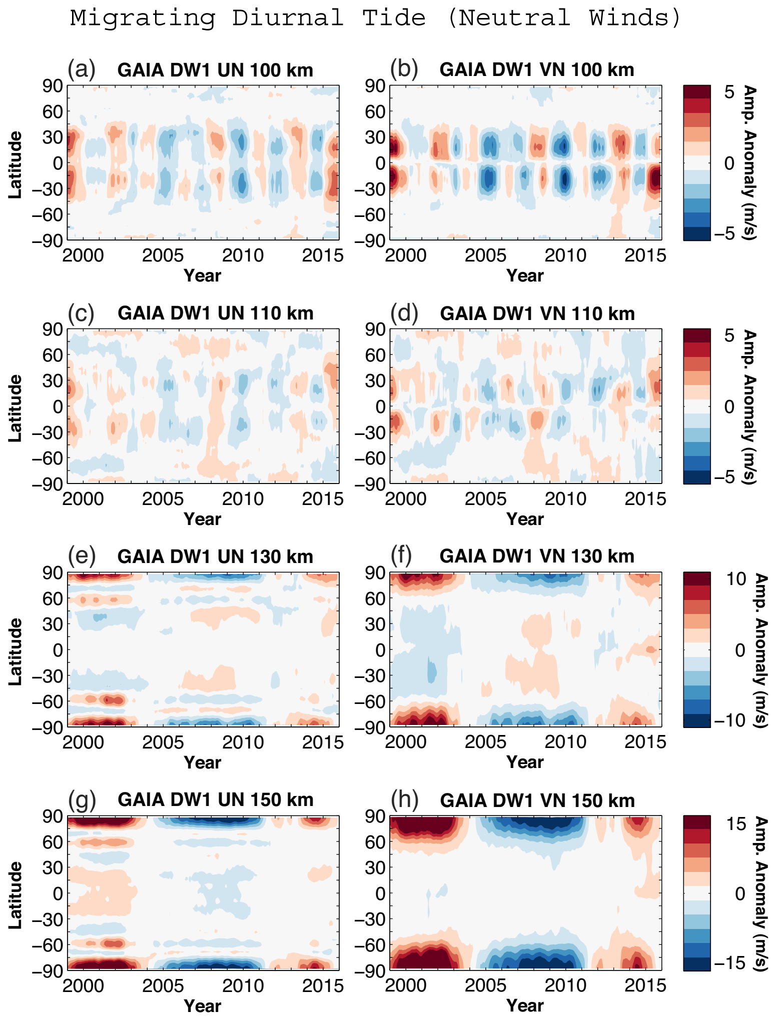

Figure 8. 13-month smoothed amplitude anomaly of $DW1$ in the (left) zonal and (right) meridional winds derived from GAIA at (a,b) 100 km, (c,d) 110 km, (e,f) 130 km, and (g,h) 150 km. It is noted that the color scale is not the same at different altitudes. (See Figure S1 in the supporting information for the seasonal climatology of $DW1$.)

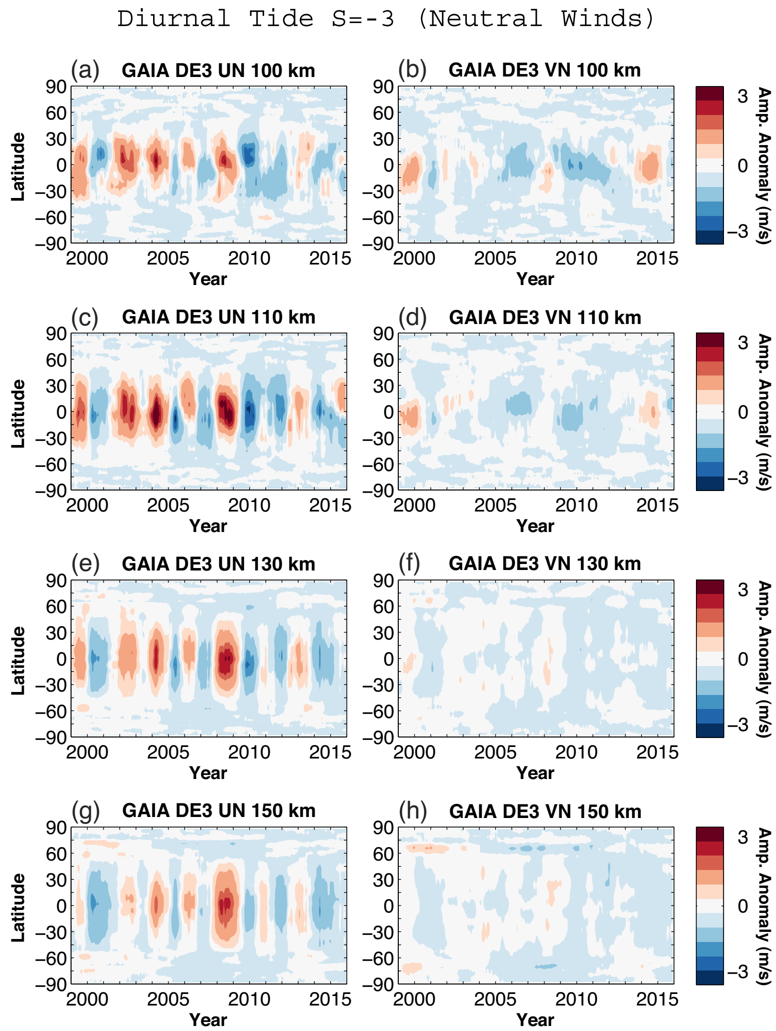

Figure 9. 13-month smoothed amplitude anomaly of $DE3$ in the (left) zonal and (right) meridional winds derived from GAIA at (a,b) 100 km, (c,d) 110 km, (e,f) 130 km, and (g,h) 150 km. (See Figure S2 in the supporting information for the seasonal climatology of $DE3$.)

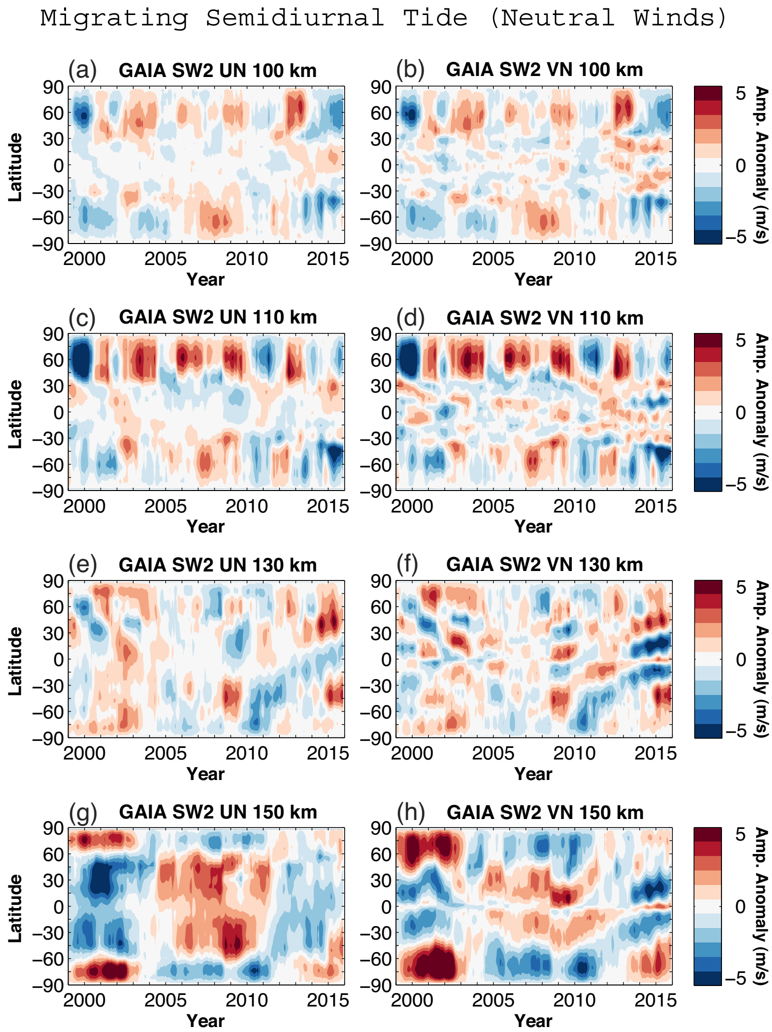

Figure 10. 13-month smoothed amplitude anomaly of $SW2$ in the (left) zonal and (right) meridional winds derived from GAIA at (a,b) 100 km, (c,d) 110 km, (e,f) 130 km, and (g,h) 150 km. (See Figure S3 in the supporting information for the seasonal climatology of $SW2$.)

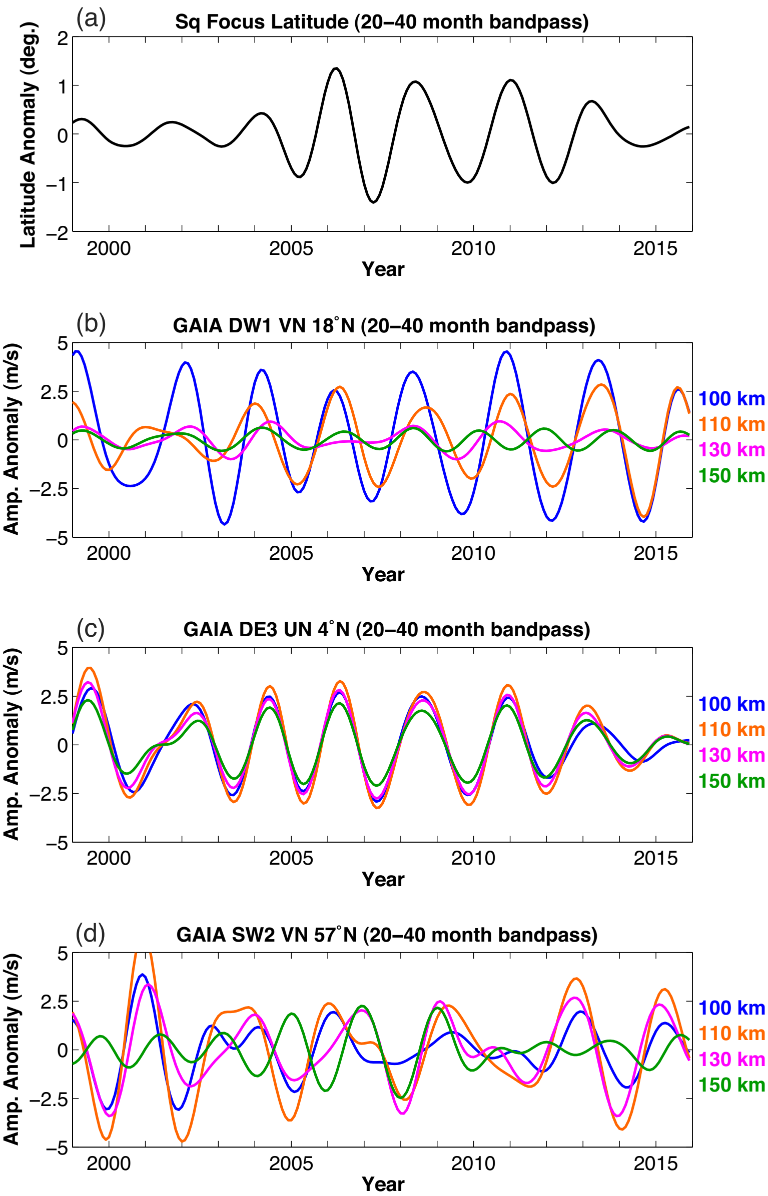

Figure 11. 20–40 month bandpass-filtered anomaly in the (a) S_q focus latitude, (b) $DW1$ meridional wind amplitude at 18°N, (c) $DE3$ zonal wind amplitude at 4°N, and (d) $SW2$ meridional wind amplitude at 57°N. In (b–d), different colors represent different altitudes.